




# Optical Arbitrary Waveform Processing of Over 100 Spatial Channels for Optical Performance Monitoring

Mitsumasa Nakajima , Member, IEEE, Kenya Suzuki , Member, IEEE, Kazunori Seno , Ryoichi Kasahara, Takashi Goh, Member, IEEE, Yutaka Miyamoto, Member, IEEE, and Toshikazu Hashimoto

(Top-Scored Paper)

**Abstract**—We developed an optical processing platform that handles over 100 space-division-multiplexed signals in the C-band. The device consists of free-space optics based on liquid crystal on silicon (LCOS) with a waveguide frontend. Thanks to the holographic wavefront modulation by the LCOS spatial light modulator, the device arbitrarily manipulates the optical amplitude and phase in the space and spectral domains simultaneously. This ability enables us to create various optical processing functions such as tunable wavelength filtering, variable optical attenuation, and flexible delay line interferometry with arbitrary spatial and wavelength channel dependence. These functions are highly suitable for large-scale optical performance monitoring (OPM). As an application, we demonstrate OPM for 100 spatial channels over the C-band. The constructed OPM can monitor not only the power spectrum but also the optical signal-to-noise ratio (OSNR) by setting different LCOS phase patterns. We achieved channel power monitoring and OSNR monitoring with 1.8- and 1.9-dB accuracy over 100 spatial channels.

**Index Terms**—Integrated optics, optical waveguides, space division multiplexing, spatial light modulators, wavelength division multiplexing.

## I. INTRODUCTION

SPACE division multiplexing (SDM) using parallel spatial paths such as multicore fibers or few mode fibers is an attractive way to enhance transmission capacity per optical fiber [1]–[3]. Recent experimental demonstrations of SDM transmission have clearly shown that SDM is promising for future backbone networks with ultra-high capacity [4]–[8]. In SDM networks, optical performance monitors (OPMs) will play an essential role, as they have done in wavelength division

multiplexing (WDM) networks, because they are the basis of many network level applications such as error diagnosis, wavelength allocation, and impairment-aware routing [9]–[13]. The OPMs for WDM signals have been realized by using a tunable wavelength filter with a single photodiode (PD). They can measure optical power for every wavelength channel by sweeping the center frequency of the filter. In addition, the optical signal to noise ratio (OSNR), a fundamental performance index of the signal quality, can be measured by installing a delay-line-interferometer (DLI) after the wavelength filter [14]–[17]. As these configurations are simple and cost-effective, they are widely used for OPMs. However, in SDM systems, a massive number of monitoring devices will be required because SDM signals are densely multiplexed in space and wavelength division. For example, in an M-degree ROADM system with N-core fiber,  $2M \times N$  units of WDM monitors are required in each node, so, for instance, 112 OPMs are required when  $M = 8$  and  $N = 7$ . In addition, the monitors will also have to be highly functional so that they can deal with different transmission formats and bandwidths.

Recently, an arbitrary optical spectral pulse processing technique, which had been developed for ultrafast pulse shaping for femtosecond lasers [18], [19], has been demonstrated for optical signal processing for telecom devices [20]–[29]. Processing technology based on a liquid-crystal-on-silicon (LCOS) spatial light modulator is highly suitable because of its flexibility [20]–[27]. Thanks to the holographic wavefront modulation by the LCOS, the device can process optical signals in spectral and time domains arbitrarily. This ability enables us to construct various devices for WDM signal processing by only updating the phase pattern on the LCOS, such as wavelength filters, variable optical attenuators (VOAs), tunable dispersion compensators, discrete Fourier domain filters, and variable delay-line-interferometers (DLIs). Owing to this feature, functional OPMs supporting multi-signal formats with a flexible passband for WDM signals have been demonstrated [15], [16]. Toward SDM signal processing using this technology, multiple spectral processors have been demonstrated in [27], [30], [31]. However, their spatial channel counts are limited to around ten. In addition, as they are only used for spectral filters, their ability in programmable waveform shaping of the SDM signals was not investigated. In this paper, we demonstrate a densely integrated programmable spectral processor supporting 120 spatial channels for arbitrary

Manuscript received July 1, 2018; revised September 3, 2018; accepted September 4, 2018. Date of publication September 14, 2018; date of current version February 20, 2019. This work was supported in part by the R&D project on “Research and Development of Space-Division Multiplexing Photonic Node” of the National Institute of Information and Communications Technology (NICT). (Corresponding author: Mitsumasa Nakajima.)

M. Nakajima, K. Suzuki, K. Seno, R. Kasahara, T. Goh, and T. Hashimoto are with Nippon Telegraph and Telephone Device Technology Laboratories, NTT Corporation, Atsugi 243-0198, Japan (e-mail: mitsumasa.nakajima.wc@hco.ntt.co.jp; kenya.suzuki.mt@hco.ntt.co.jp; kazunori.seno.ur@hco.ntt.co.jp; ryoichi.kasahara.fs@hco.ntt.co.jp; takashi.goh.ue@hco.ntt.co.jp; toshikazu.hashimoto.ur@hco.ntt.co.jp).

Y. Miyamoto is with Nippon Telegraph and Telephone Network Innovation Laboratories, NTT Corporation, Yokosuka 239-0847, Japan (e-mail: yutaka.miyamoto.fb@hco.ntt.co.jp).

Color versions of one or more of the figures in this paper are available online at <http://ieeexplore.ieee.org>.

Digital Object Identifier 10.1109/JLT.2018.2869895

waveform processing of SDM signals [32]. The number of spatial channels is ten times larger than in previous reports [27], [30], [31]. As an application, we demonstrate the first integrated OPM for SDM network using the proposed device.

## II. DEVICE STRUCTURE AND OPERATIONAL PRINCIPLE

### A. Over 100 Spatial-Channel Spectral Processor

The key technology for arbitrary waveform processing of the SDM signal is a multilane photonic spectral processor on a spatial and planar optical circuit (SPOC) platform that combines waveguides and free-space optics [24], [25], [27], [32]–[36]. Fig. 1(a) is an explanatory schematic of the proposed spectral processor array on the SPOC platform. Fig. 2(a) and (b) show the lane-multiplexing ( $y$ - $z$ ) and dispersion ( $x$ - $z$ ) planes of the optics. The device consists of a waveguide frontend, a diffractive grating, lenses, and LCOS. In addition, we employed polarization diversity optics [a polarization beam splitter (PBS) and half-wave plate (HWP)] between the collimating lens and the grating because LCOS is polarization dependent. In these optics, the signals from the fiber array are input to the waveguide frontend, where the input beams are enlarged and multiplexed by a spatial beam transformer (SBT). The structure of the SBT is illustrated in the Fig. 2(a). The SBT consists of input/output (I/O) waveguides, a slab waveguide, and arrayed waveguides. It has basically the same circuit structure as an arrayed waveguide grating (AWG), except that the path length difference of the arrayed waveguides is set at zero. It therefore does not disperse the light spectrally but rather forms an output beam profile. At the facet of the waveguide, the beams go at different angles because their wavefront is different. They are focused on different areas of the LCOS plane by the Fourier lens. Thus, each signal from the input ports can be handled separately. Each one is spatially modulated by encoding a wavefront using the LCOS, and they return to the output ports in the waveguide. Thanks to the software-upgradable spatial optical modulation by LCOS, the device arbitrarily manipulates the optical amplitude or phase for each spatial ( $y$ -direction) and wavelength channel ( $x$ -direction) individually. Thus, the processor can provide various functions through each signal, as shown in Fig. 1(b).

Using a similar configuration, we have already demonstrated seven arrayed wavelength filters for gain equalizing of seven-core fibers [27]. Here, we investigate the maximum spatial count of this system. The maximum number of spatial channels ( $M$ ) is simply determined by the following equation;

$$M = H/d_{\text{LCOS}}, \quad (1)$$

where  $H$  is the height of LCOS and  $d_{\text{LCOS}}$  is the beam separation on it. To suppress the crosstalk (XT) between neighboring ports, ( $d_{\text{LCOS}}$ ) should be set larger than the beam radius on the LCOS ( $\omega_{\text{LCOS}}$ ). By considering Gaussian beam propagation, the XT can be estimated as

$$XT = \exp \left\{ - \left( \frac{d_{\text{LCOS}}}{\omega_{\text{LCOS}}} \right)^2 \right\} \quad (2)$$

From eq. (2),  $d_{\text{LCOS}}$  should be set larger than  $3.7 \times \omega_{\text{LCOS}}$  to obtain a low XT value of  $< -60$  dB. Thus,  $M$  becomes

large as  $\omega_{\text{LCOS}}$  becomes smaller. However, it becomes difficult to construct the DLI function when the  $\omega_{\text{LCOS}}$  becomes small. (The DLI function is the key to realizing an OSNR monitor, as described later). To utilize the LCOS with the highest efficiency, we investigated the minimum beam radius on the LCOS ( $\omega_{\text{LCOS}}$ ) for constructing the DLI function. By considering Gaussian beam propagation, we found  $\omega_{\text{LCOS}} = 9$  pixels is the smallest beam radius for constructing it with a good extinction ratio of over 20 dB. Thus, the minimum  $d_{\text{LCOS}}$  value is 33.5 pixels. Fig. 1(c) shows the possible  $M$  values as a function of pixel number of LCOS with a  $d_{\text{LCOS}}$  value of 33.5 pixels. For comparison, the case for a  $d_{\text{LCOS}}$  value of 140 pixels is also plotted, which is the value in our previous work [27]. The reported  $M$  values from previous work are also plotted [27], [30], [31]. As can be seen in this figure, the  $M$  value becomes about four times larger than in the previous study with the same number of pixels. In addition, when we utilize 4K-LCOS, which has 4096 pixels along the longitudinal direction, we can arrange 120 spatial channels onto the LCOS display. The number of spatial channels is ten times larger than in previous reports.

We designed the optics to achieve such a beam arrangement. In the SPOC optics, the beam radius  $\omega_{\text{LCOS}}$  and beam position  $d_{\text{LCOS}}$  on the LCOS can be described as follows under the small angle approximation by considering simple  $2$ - $f$  Fourier optics [27], [33]:

$$\omega_{\text{LCOS}} = f_o \lambda / \pi \omega_{\text{SBT}} \quad (3)$$

$$d_{\text{LCOS}} = f_o \theta_{\text{SBT}}, \quad (4)$$

where  $f_o$  is the focal length of the lens,  $\lambda$  is the optical signal wavelength in vacuum,  $\omega_{\text{SBT}}$  is the beam radius on the SBT, and  $\theta_{\text{SBT}}$  is the output angle from the chip facet. Thus, we can control  $\omega_{\text{LCOS}}$  and  $d_{\text{LCOS}}$  by designing parameters  $\omega_{\text{SBT}}$  and  $\theta_{\text{SBT}}$ . They are designed by using the following relationships:

$$\omega_{\text{SBT}} = \frac{f_{\text{SBT}} \lambda d_2}{\pi \omega_o d_1}, \quad (5)$$

$$\theta_{\text{SBT}} = \frac{p d_2}{f_{\text{SBT}} d_1}, \quad (6)$$

where  $n$  is the effective refractive index of the slab waveguide,  $\omega_o$  is the beam radius of the eigen mode of the input waveguide,  $d_1$  and  $d_2$  are the periods of the arrayed waveguides at the junction of the slab waveguide and the chip facet,  $p$  is the period of the input waveguide at the input side of the slab waveguide, and  $f_{\text{SBT}}$  is the focal length of the slab waveguide. As can be seen in eqs. (3) and (5), a dense beam arrangement on the LCOS requires a relatively large footprint of the waveguide front. This typically affects fabrication errors, which cause fringing of the optical field in the slab waveguides and neighboring-channel XT. To suppress this XT, we arrange the I/O ports alternately as shown in Fig. 2(a).

### B. Optical Arbitrary Waveform Processing by LCOS

The LCOS can display a quantized multi-level phase pattern that spatially modulates the wavefront of an input optical beam. Thanks to its high spatial resolution and software upgradable feature, we can construct various devices by setting a different

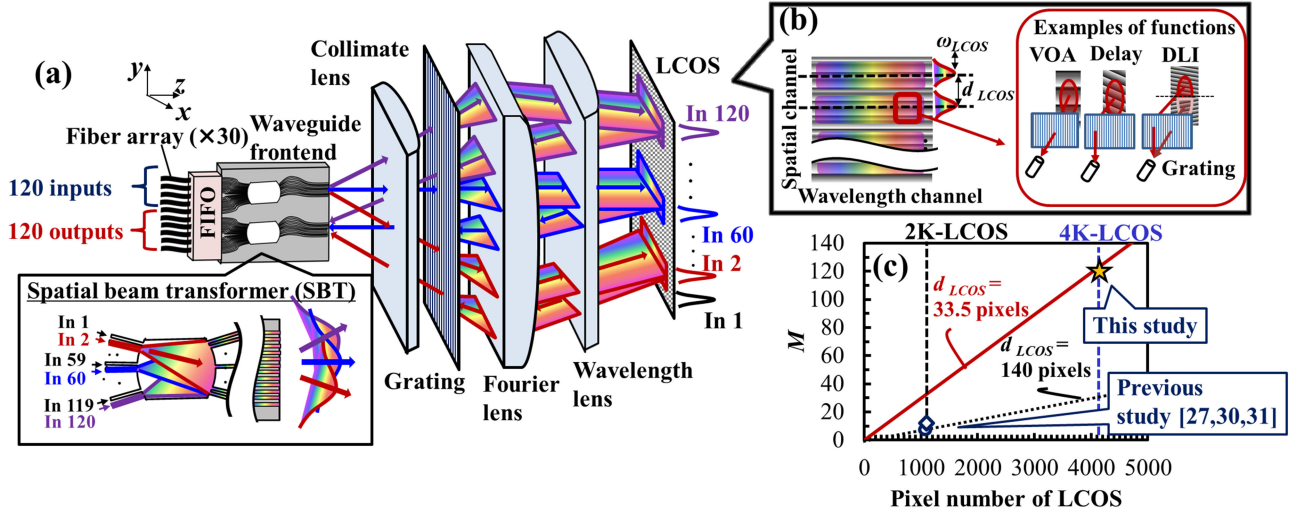


Fig. 1. (a) Schematic diagram of 120-spatial-channel-multiplexed spectral processor. (b) Displayed phase pattern on LCOS and examples of their function. (c) Spatial channel count ( $M$ ) as a function of pixel number of LCOS.

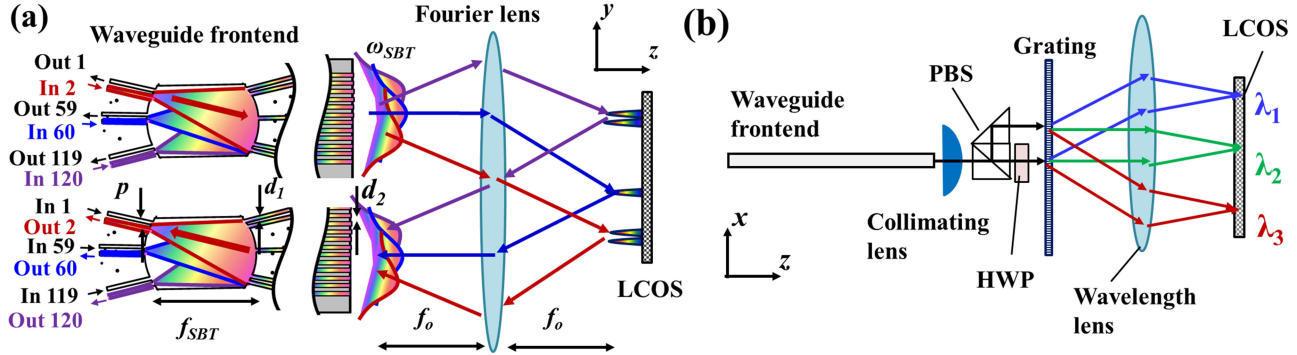


Fig. 2. (a)  $y$ - $z$  plane and (b)  $x$ - $z$  plane for the proposed 120-spatial-channel-multiplexed spectral processor.

phase pattern for each spatial and wavelength channel. For example, we can set a different attenuation value for each channel by displaying the blazed phase pattern along the  $y$ -axis on the LCOS. The attenuation ratio (ATT) is determined by the following equation:

$$ATT = \exp \left\{ - \left( \frac{\pi \omega_{LCOS}}{\lambda} \theta_{LCOS} \right)^2 \right\}, \quad (7)$$

where  $\theta_{LCOS}$  is the steering angle along the  $y$ -direction from the LCOS, which can be controlled by the slope of the blazed phase. Using this function, we can construct a spatially multiplexed tunable wavelength filter.

The processor can also control the signals in the time domain by setting the phase pattern along the  $x$ -direction on the LCOS. For example, when we set the linear phase slope along the  $x$ -direction on the LCOS, we can construct a tunable delay line thanks to the large path difference arising from the grating. The group delay  $\tau_o$  of this system is expressed as follows [16], [23], [25]:

$$\tau_o = \frac{\lambda^2}{2\pi c D} \frac{d\Phi_{LCOS}(x, y)}{dx} = \frac{k\lambda^2}{2\pi c D}, \quad (8)$$

where  $\phi_{LCOS}$  is the phase pattern added to the SLM,  $\omega$  is the angular frequency,  $\lambda$  is the wavelength,  $x$  is the position along the dispersion axis on the SLM,  $D$  is the linear dispersion of the grating on the SLM ( $D = d\lambda/dx$ ), and  $c$  is the speed of light. Typically,  $\tau_o$  can be controlled on a picosecond order. Note that the wavelength dispersion can be emulated by setting a nonlinear phase profile along the  $x$ -direction [23], [25].

Using the delay functions, the DLI can also be constructed [15], [16], [22]. In this configuration, the displayed area on the LCOS is divided into two areas. The patterns on these areas are the blazed waveforms with the same period but with the opposite sign in the axis of the dispersion of the diffraction grating ( $x$ -direction). Thus, the incident beams are separately phase-modulated, deflected, and reflected at the diffraction angles back to the input/output frontend with different paths. Thanks to the difference in the path length of the reflected lights, the DLI function can be realized. When we set the phase slope of both areas on the SLM to  $k$  and  $-k$ , we can construct the DLI with a relative delay length  $\tau$  of  $2\tau_o$ . In addition, a phase offset  $\varphi_o$  is added on the upper side of the separated area on the LCOS in order to tune the phase shift slightly. More complex interferometric operation can be achieved by splitting optical beams much more.

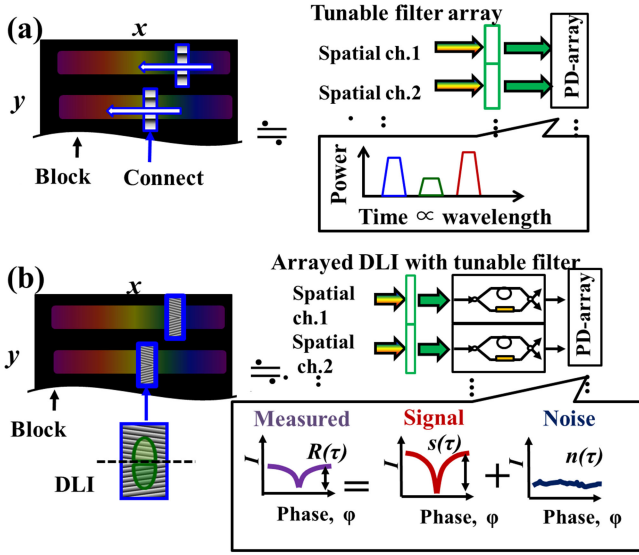


Fig. 3. Method for measuring (a) channel power and (b) OSNR for SDM signals.

### C. Operational Principle of OPM

A possible application of this device is an SDM-compatible OPM. Among the various performance indexes of optical signal quality, the optical channel power and OSNR are the important ones because they are directly related to the signal bit error rate (BER) [37]. Fig. 3(a) explains the method for observing the channel power using the proposed processor. The channel power for WDM signals has been realized by using a tunable wavelength filter with a single photodiode (PD). The optical power can be measured for every wavelength channel by sweeping the center frequency of the filter. The block pattern in Fig. 3(a) can be achieved by using a large steering angle pattern, e.g., a binary phase grating pattern along the  $y$ -direction with a period of 2 pixels. As the PD array has a single PD per fiber, our device can independently set the tunable filter for each spatial channel. Thus, we can simultaneously measure the channel power for SDM by connecting the PD array to multiple output ports.

The OSNR measurements for SDM signals were conducted by using the same configuration with the DLI function. Fig. 3(b) explains the method for estimating the OSNR using the proposed processor. By using the DLI, an OSNR can be estimated from the difference in the interfered powers between the signal and noise. With this technique, the OSNR is estimated as [14], [15]:

$$OSNR(dB) = 10 \log_{10} \left( \frac{\Delta\nu}{0.1 \text{ nm}} \left[ \frac{(n+1)(s-n)}{(R-n)(s+1)} - \frac{n+1}{s+1} \right]^{-1} \right), \quad (9)$$

where  $s$  (and  $n$ ) is the calibration parameter, which is defined as the power ratio between the constructive and destructive interference conditions when there is no noise (and no signal).  $\Delta\nu$  is the noise equivalent bandwidth (typically the channel bandwidth) and  $R$  is the observed power ratio between the constructive and destructive interference conditions. As the calibration parameters ( $s$  and  $n$ ) are determined by the coherence of the signal and noise, they only require one measurement.

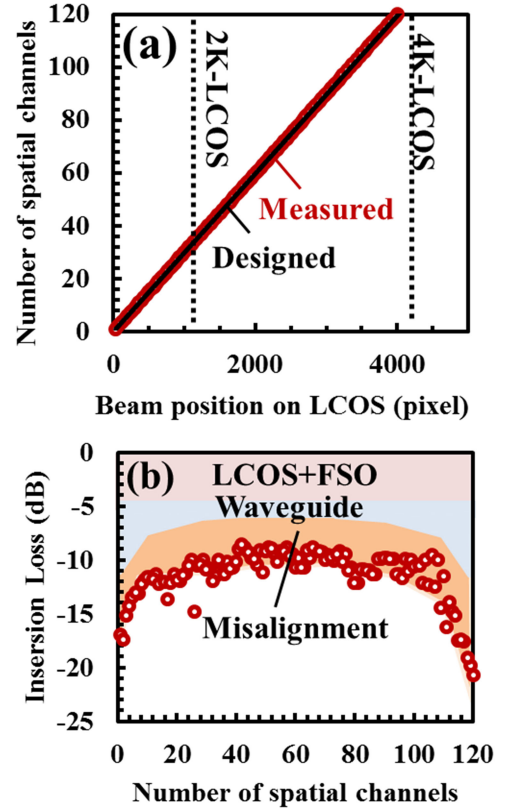


Fig. 4. (a) Measured and observed beam position on the LCOS. (b) Transmittance as a function of spatial channel.

The DLI is reconfigurable through the wavefront modification by LCOS, which enables us to optimize the delay line length on demand (the optimization is described in the following section). Hence, other techniques for OSNR monitoring have been proposed, such as polarization nulling, nonlinear effects, waveform sampling, and neural-network-based machine learning [38]–[41]. In particular, the DLI-based approach is very promising because it is simple and intrinsically insensitive to both chromatic dispersion and polarization mode dispersion and the signal formats [14]–[17]. This feature is rather attractive for monitoring of recent polarization-multiplexed SDM signals.

### III. FABRICATION AND DEVICE CHARACTERISTICS

As a demonstration, we constructed an optical bench-top for the 120-array photonic spectral processor using the SPOC platform. The waveguide frontend was fabricated by using a conventional silica-based planar lightwave circuit (PLC) with an index contrast of 1.5%. The red line in Fig. 4(a) shows the measured beam position on the LCOS. The observed beam profiles of 16-input ASE spectra are shown in the inset. As shown in the figure, the designed optical beams are realized. Fig. 4(b) shows the transmittance of the fabricated optical bench-top. The insertion loss (IL) ranged from 8.5 to 14.8 dB for the center 100 spatial channels, but that of the 20 edge ports reached 22 dB. The loss budgets, shown in Fig. 4(b) include a waveguide loss of 1.5 to 5.5 dB, grating loss of 2.5 dB, LCOS loss of 1.3 dB including diffraction loss, free-space optics loss of 0.4 dB (including the polarization beam splitter loss), and alignment loss

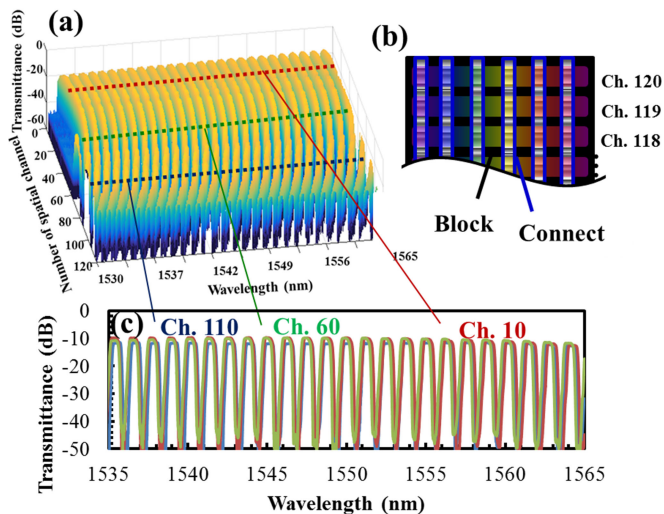


Fig. 5. (a) Transmittance spectra filtered by 100-GHz grid. (b) Displayed phase pattern on LCOS. (c) Measured spectra for spatial channel 10, 60, and 110.

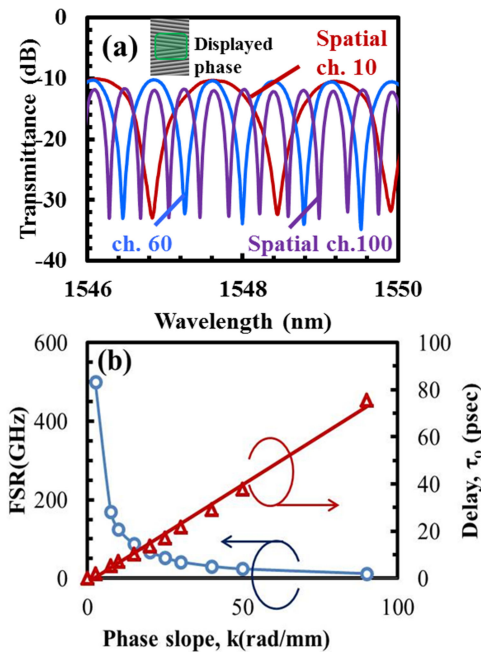


Fig. 6. (a) Transmittance spectra of DLI filter with different delay for each spatial channel. (b) FSR and delay as a function of phase slope along dispersion axis.

of 3 to 5 dB. The loss increment of the waveguide is due to the free spectral range of the SBT, which can be suppressed by employing a narrower waveguide pitch at the facet. By optimizing the grating and waveguide, we can reduce IL to less than 8 dB.

Fig. 5(a) shows the transmission spectra with a passband width of a 100-GHz grid for 120 spatial channels. The displayed phase pattern on the LCOS is shown in Fig. 5(b). The enlarged spectra for spatial channel 10, 60, and 110 are shown in Fig. 5(c). As shown in the figure, the signal of all spatial channels can be shaped by using the phase pattern on the LCOS. The wavelength isolation was typically less than  $-40$  dB. The interspatial-channel XT was typically less than  $-30$  dB. Fig. 6(a)

shows typical observed interference spectra from the DLI patterns with various delay times. The extinction ratio of  $\sim 20$  dB was good for all of the examined spatial channels, which suggests that it can be used for OSNR monitoring. We estimated the delay from the measured free spectral range (FSR). The results are shown in Fig. 6(b). The obtained optical delay was proportional to the  $k$  value and tuned from 0 to about 80 ps, which agrees with the expectation from eq. (6). These results suggest the successful operation of the arbitrary waveform processing function of the device.

#### IV. APPLICATION TO PERFORMANCE MONITORING

##### A. Experimental Setup

To confirm that our device is applicable to SDM signal monitoring, we demonstrated an OPM for multiple signal inputs. Fig. 7(a) shows a schematic of the experimental configuration. In this experiment, we examined the center 100 spatial channels. We used two experimental setups: one for OSNR monitoring of 100-Gbps DP-QPSK signal with a 28-Gbaud rate with a carrier wavelength of 1550 nm, and the other for power monitoring of ASE spectra filtered by a wavelength selective switch (WSS) with a 50-GHz passband. The reference power and OSNR value were swept by using the VOAs and amplifier gain, and the real power and OSNR were confirmed with a commercial optical spectral analyzer (OSA). Both signals were split and amplified and then connected to the odd and even ports of the proposed device, respectively. The output signals were monitored by a PD array at the same time. To realize the OPM functions, we set the phase pattern on the LCOS as shown in Fig. 7(b). The filtering pattern was swept along the x-axis in the even spatial channels in order to measure the filtered ASE spectra. On the other hand, we did not scan the filtering pattern in the odd spatial channels because only the 1550-nm-wavelength channel was examined for OSNR monitoring.

##### B. Power Monitoring

To measure the wavelength dependence of the input power, we set the bandpass filter (BPF) pattern on the LCOS and swept the center frequency of the filter. The filtering bandwidth (BW) was set to 12.5 GHz, and the step of the center frequency was set to 6.25 GHz. By considering the insertion loss and background noise including XT, we can estimate the spectrum of the input signals from the PD's time dependence. Fig. 8(a) and (b) show typical measured optical power spectra observed in spatial channel 60. For comparison, the spectrum measured by a commercial OSA is also shown. The estimation error was less than 0.5 dB in this spatial channel. The measurement took about one minute per C-band scan, which was due to the time response of the liquid crystal (on the order of 100 ms). The measurement time can be improved by using fast SLMs such as micro-mirror based ones.

Next, we checked the spatial channel dependence of the input power. We set the BW of the filter to 50 GHz and measured the optical power of the center wavelength channel (1550 nm) as a function of spatial channels. The results are shown in Fig. 8(c).

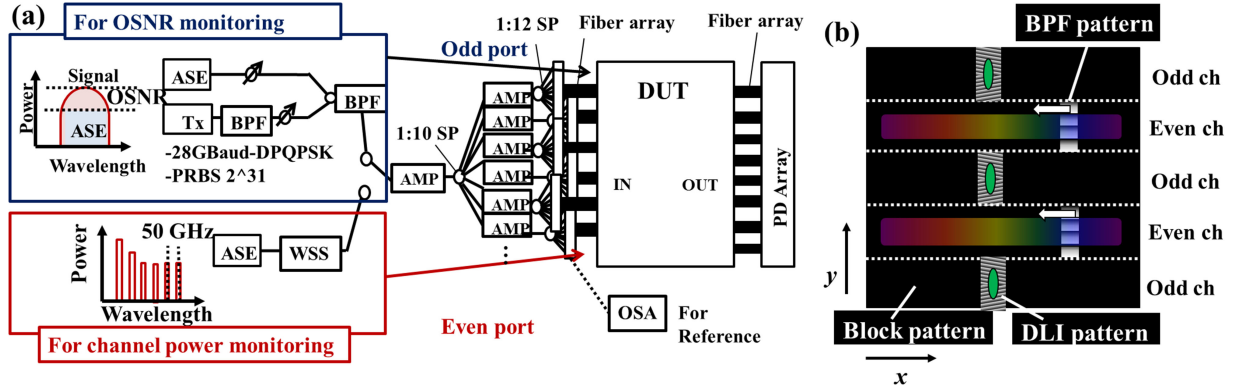


Fig. 7. (a) Schematic of experimental set up. (b) Displayed phase pattern on LCOS for OPM demonstration.

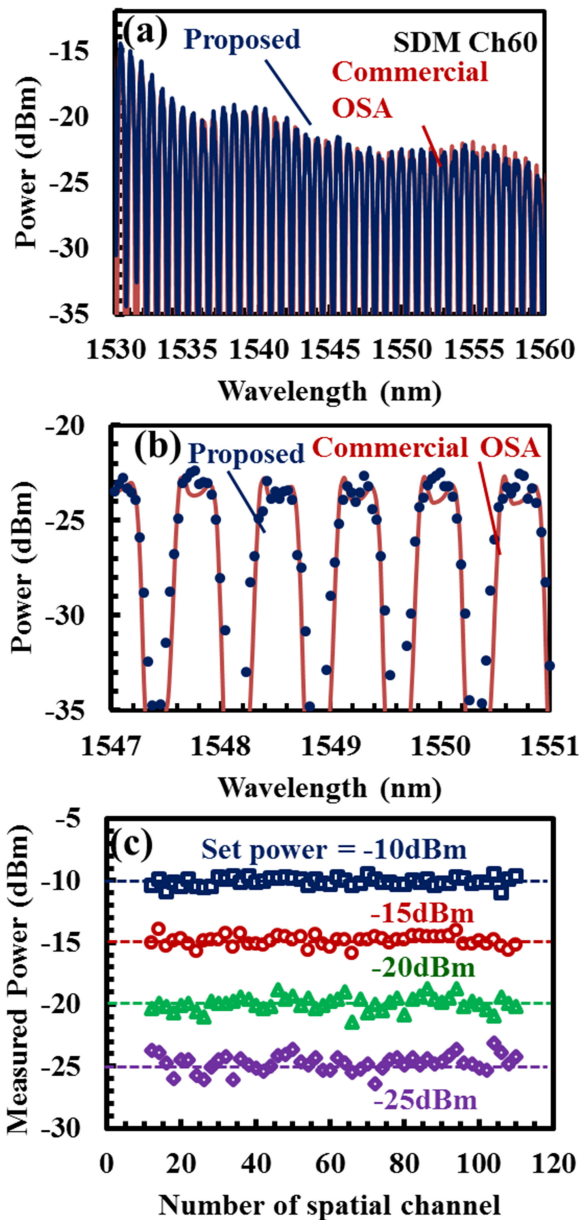


Fig. 8. (a), (b) Measured and reference spectra for spatial channel 60. (c) Estimated channel power as a function of spatial channel.

The accuracies are  $\pm 0.5$  and  $\pm 1.8$  dB at the input power of  $-10$  and  $-25$  dBm.

### C. OSNR Monitoring

In a DLI-based OSNR monitor, the delay time between the two interferometric arms significantly affects monitoring performance, which requires precise tuning of the delay length by considering the transmitted signal parameters [17]. In addition, the filtering shape of the BPF in front of interferometer should be optimized to accurately measure the OSNR for high-speed signals [42], [43]. Thanks to the programmable feature of the proposed DLI, we can optimize the  $\tau$  value in the DLI and the filtering shapes of the wavelength filter by simply changing the displayed phase pattern on the LCOS. However, to our knowledge, how this parameter can be optimized using a LCOS-based spectral processor is not well understood. Thus, we first describe their optimizations for OSNR monitoring.

For increasing the accuracy of the OSNR monitor, the  $s$  and  $n$  values in eq. (9) are important. These parameters significantly depend on the delay time in a DLI arm because of the difference in coherence. By using the coherence function,  $s$  and  $n$  can be described by the following equations:

$$s = \frac{1 + |\gamma_s(\tau)|}{1 - |\gamma_s(\tau)|} \quad (10)$$

$$n = \frac{1 + |\gamma_n(\tau)|}{1 - |\gamma_n(\tau)|} \quad (11)$$

where  $\gamma_s(\tau)$  and  $\gamma_n(\tau)$  are the coherence (or autocorrelation) function of the signal and the noise, and  $\tau$  is the delay time in the DLI. To increase the accuracy of the OSNR monitor, the  $n$  value should be small, which means that  $\tau$  should be selected to minimize  $\gamma_n(\tau)$ . Generally,  $\gamma_s(\tau)$  and  $\gamma_n(\tau)$  are Fourier transforms of the power spectra of the signal  $S(\omega)$ , as shown in Fig. 9(a) and (b). Therefore, when a filtered signal is introduced into the DLI,  $\gamma_s(\tau)$  shows a gently sloped dependence, as indicated by the black line in Fig. 9(a). On the other hand, when unfiltered noise with a wide and flat spectrum is introduced into the DLI,  $\gamma_n(\tau)$  immediately drops to zero with increasing  $\tau$ , as shown by the blue line in Fig. 9(b). However, as the noise is usually filtered by WDM filters,  $\gamma_n(\tau)$  becomes

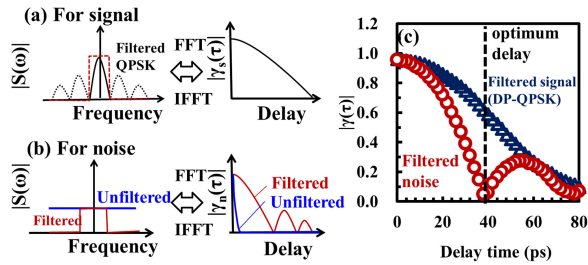


Fig. 9. Schematic of relationships between coherence functions and power spectra for (a) signal and (b) noise. (c) Experimentally obtained coherence functions for filtered 100-Gbps DP-QPSK signal and noise.

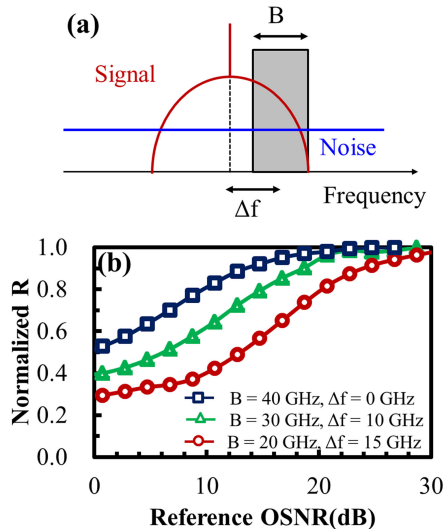


Fig. 10. (a) Schematic of narrow bandwidth filtering in frequency domain. (b) Normalized observed power ratio between the constructive and destructive interference conditions as a function of OSNR value.

sinc-shaped, as shown by the red line in Fig. 9(b). In this case, the delay time should be chosen as the null point in  $\gamma_n(\tau)$  to enhance the sensitivity of the OSNR monitors. In the case of the proposed DLI, we can tune the value of  $\tau$  by changing the displayed phase slope on the LCOS. Therefore, the null point can be directly estimated by observing  $\gamma_n(\tau)$ . As  $\gamma_n(\tau)$  typically depends on the filtering shape of a node device such as a wavelength selective switch, it has been difficult to determine the accurate OSNR value in practical dynamic ROADMs systems using the conventional DLI-based OSNR monitor. On the other hand, the proposed method enables direct measurement of  $\gamma_n(\tau)$ . In addition, we can tune the optimum delay value to eliminate the accuracy degradation. Therefore, this method can be employed even in a dynamic ROADM system. For a demonstration of this function, we experimentally measured  $\gamma_n(\tau)$  and  $\gamma_s(\tau)$  using an ASE source and 100-Gbps DP-QPSK signals. The experimental setup is the same as the one in Fig. 7(a). In this experiment, the signal and noise were filtered by a 40-GHz bandpass filter. The results are shown in Fig. 9(c). As shown in the figure,  $\gamma_n(\tau)$  shows a sinc-shaped function as expected. On the other hand,  $\gamma_s(\tau)$  shows gently sloped dependence, which reflects the Gaussian-like power spectra of the filtered signals.

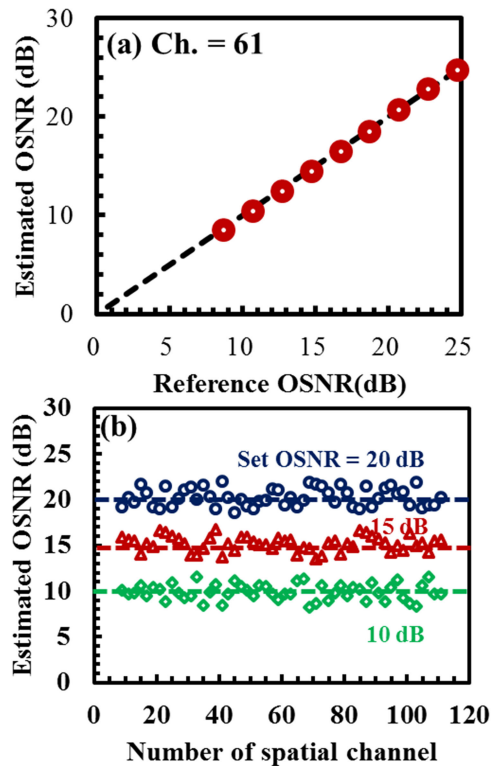


Fig. 11. (a) Estimated OSNR as a function of reference OSNR for spatial channel 61. (b) Estimated OSNR value as a function of spatial channel number.

From the null point of the sinc-shaped  $\gamma_n(\tau)$ , we determined the optimum delay time to be 37 ps in this case.

In order to measure the OSNR for high-speed signals accurately with a practical dynamic range using a DLI-based monitor, a tunable band-pass filter with a narrow bandwidth must be put in front of interferometer [42], [43]. In this approach, the center frequency of the filter should be detuned from the signal carrier frequency to extract a part of the noisy signal spectrum at those frequencies, as shown in Fig. 10(a). Then, the signal spectrum approaches the noise spectrum, which makes the contribution of the noise larger. The proposed DLI also supports this function because a filtered spectrum can be tuned by changing the displayed area on the LCOS.

For the validation of this method, we investigated the dependence of the interference on the filtering shape by using 100-Gbps DP-QPSK signals and an ASE source. Fig. 10(b) shows the change in the observed normalized  $R$  value with various filtering bandwidths  $B$  and filtering center offsets  $\Delta f$  as a function of the reference OSNR. The reference OSNR value was swept by changing the signal power with a variable optical attenuator. As can be seen in Fig. 10(b), the  $R$  curve shifts to the higher OSNR region when the filtering center offset becomes large. This means that the sensitive range can be tuned by pre-tuning the filtering shapes. By considering the preferred dynamic range of OSNR monitoring (typically 10–25 dB), we can optimize the filtering shapes.

By using the above methods, the OSNR values were estimated for SDM channels. In this experiment, the center wavelength channels (1550 nm) were examined. The  $\tau$  value of the

DLI was determined to 37 ps by observing the coherence function of noise. The filtering shapes were set to  $B = 20$  GHz and  $\Delta f = 15$  GHz for the DP-QPSK signal to maximize the monitoring sensitivity. Fig. 11(a) shows the OSNR estimated from eq. (9) as a function of the real OSNR value for spatial channel 61. The measured OSNR error is less than 0.4 dB in the range of 10 to 25 dB. Note that the estimation error was larger than 5 dB when the pre-calibration described above was not employed. Fig. 11(b) shows the measured OSNR as a function of spatial channels. The worst measured accuracies are  $\pm 1.9$  dB over  $-10$  to  $-20$  dB, which were degraded from the center channel. The accuracy mainly depends on the calibration errors because we use the same filtering shape and delay for all spatial channels. The calibration error is mainly caused by non-uniform filtering characteristics along the spatial channel of the constructed prototype devices. This non-uniformity is not an essential issue, and we can suppress the spatial channel dependency much more by optimizing the alignment method and design of the free-space optics. Thus, we believe that the degradation of accuracy can be suppressed by improving the optics and the calibration method in the future.

## V. CONCLUSION

We demonstrated a densely integrated programmable spectral processor supporting 120 spatial channels for arbitrary waveform processing of SDM signals. The number of spatial channels is ten times larger than in previous reports. Thanks to the holographic wavefront modulation by the LCOS spatial light modulator, the device arbitrarily manipulates the optical amplitude or phase in space and spectral domains simultaneously. As an application, we demonstrated the first integrated OPM for the SDM network using the proposed device. The constructed OPM can monitor not only the power spectrum but also the optical signal to noise ratio (OSNR) by setting different LCOS phase patterns. We achieved channel power monitoring and OSNR monitoring with 1.8- and 1.9-dB accuracy over 100 spatial channels.

## ACKNOWLEDGMENT

The authors would like to thank Dr. Joji Yamaguchi, Mr. Keita Yamaguchi, Mr. Naru Nemoto, and Mr. Mitsunori Fukutoku for fruitful discussions.

## REFERENCES

- [1] I. Tomkos, Y. Miyamoto, G. Wellbrock, and P. J. Winzer, "Spatially and spectrally flexible elastic optical networking," *IEEE Commun. Mag.*, vol. 53, no. 2, pp. 20–22, Feb. 2015.
- [2] T. Morioka, "New generation optical infrastructure technologies: EXAT initiative towards 2020 and beyond," in *Proc. Optoelectron. Commun. Conf.*, Hong Kong, 2009, Paper FT4.
- [3] P. J. Winzer, "Optical networking beyond WDM," *IEEE Photon. J.*, vol. 4, no. 2, pp. 647–651, Apr. 2012.
- [4] T. Kobayashi *et al.*, "1-Pb/s (32 SDM/46 WDM/768 Gb/s) C-band dense SDM transmission over 205.6-km of single-mode heterogeneous multi-core fiber using 96-Gbaud PDM-16QAM channels," in *Proc. Opt. Fiber Commun. Conf.*, Los Angeles, CA, USA, 2017, Paper Th5B.1.
- [5] T. Mizuno, H. Takara, K. Shibahara, A. Sano, and Y. Miyamoto, "Dense space division multiplexed transmission over multicore and multimode fiber for long-haul transport systems," *J. Lightw. Technol.*, vol. 34, no. 6, pp. 1484–1493, Mar. 2016.
- [6] K. Shibahara, T. Mizuno, D. Lee, and Y. Miyamoto, "Processing techniques enabling long-haul dense SDM transmissions," *J. Lightw. Technol.*, vol. 36, no. 2, pp. 336–348, Jan. 2018.
- [7] B. J. Puttnam *et al.*, "2.15 Pb/s transmission using a 22 core homogeneous single-mode multi-core fiber and wideband optical comb," in *Proc. Eur. Conf. Exhib. Opt. Commun.*, Valencia, Spain, 2015, Paper PDP.3.1.
- [8] R. Ryf *et al.*, "10-mode mode-multiplexed transmission over 125-km single-span multimode fiber," in *Proc. Eur. Conf. Exhib. Opt. Commun.*, Valencia, Spain, 2015, Paper PDP.3.3.
- [9] S. Oda *et al.*, "Optical performance monitoring for dynamic and flexible photonic networks," *Proc. SPIE*, vol. 9388, pp. 1–9, 2015.
- [10] Z. Dong, F. N. Khan, Q. Sui, K. Zhong, C. Lu, and A. P. T. Lau, "Optical performance monitoring: A review of current and future technologies," *J. Lightw. Technol.*, vol. 34, no. 2, pp. 525–543, Jan. 2016.
- [11] S. Azodolmolky, M. Klinkowski, E. Marin, D. Careglio, J. Solé Pareta, and I. Tomkos, "A survey on physical layer impairments aware routing and wavelength assignment algorithms in optical networks," *Comput. Netw.*, vol. 53, pp. 926–944, 2009.
- [12] Y. Li *et al.*, "Transparent software-defined exchange (tSDX) with real-time OSNR-based impairment-aware wavelength path provisioning across multi-domain optical networks," in *Proc. Opt. Fiber Commun. Conf.*, Los Angeles, CA, USA, 2017, Paper Th5A.2.
- [13] T. Tanaka *et al.*, "Demonstration of single-mode multicore fiber transport network with crosstalk-aware in-service optical path control," *J. Lightw. Technol.*, vol. 36, no. 7, pp. 1451–1457, Apr. 2018.
- [14] Z. Tao, Z. Chen, L. Fu, D. Wu, and A. Xu, "Monitoring of OSNR by using a Mach-Zehnder interferometer," *Microw. Opt. Technol. Lett.*, vol. 30, no. 1, pp. 63–65, Jul. 2001.
- [15] J. Schröder, O. Brasier, T. D. Vo, M. A. F. Roelens, S. Frisken, and B. J. Eggleton, "Simultaneous multi-channel OSNR monitoring with a wavelength selective switch," *Opt. Express*, vol. 18, pp. 22299–22304, 2010.
- [16] M. Nakajima, N. Nemoto, K. Yamaguchi, J. Yamaguchi, K. Suzuki, and T. Hashimoto, "In-band OSNR monitors comprising programmable delay line interferometer integrated with wavelength selective switch by spatial and planar optical circuit," in *Proc. Opt. Fiber Commun. Conf.*, Anaheim, CA, USA, 2016, Paper Th2A.11.
- [17] Z. J. Qiu *et al.*, "Guideline of choosing optical delay time to optimize the performance of an interferometry-based in-band OSNR monitor," *Opt. Lett.*, vol. 41, pp. 4178–4181, 2016.
- [18] A. M. Weiner, "Ultrafast optical pulse shaping: A tutorial review," *Opt. Commun.*, vol. 284, pp. 3669–3692, 2011.
- [19] E. Frumker and Y. Silberberg, "Femtosecond pulse shaping using a two-dimensional liquid-crystal spatial light modulator," *Opt. Lett.*, vol. 32, pp. 1384–1386, 2007.
- [20] X. Yi, T. X. H. Huang, and R. A. Minasian, "Tunable and reconfigurable photonic signal processor with programmable all-optical complex coefficients," *IEEE Trans. Microw. Theory Techn.*, vol. 58, no. 11, pp. 3088–3093, Nov. 2010.
- [21] J. Schröder, M. A. F. Roelens, L. B. Du, A. J. Lowery, S. Frisken, and B. J. Eggleton, "An optical FPGA: Reconfigurable simultaneous multioutput spectral pulse-shaping for linear optical processing," *Opt. Express*, vol. 21, no. 1, pp. 690–697, 2013.
- [22] G. N. Baxter *et al.*, "Highly programmable wavelength selective switch based on liquid crystal on silicon switching elements," in *Proc. Opt. Fiber Commun. Conf.*, Anaheim, CA, USA, 2006, Paper OTuF2.
- [23] M. A. F. Roelens *et al.*, "Dispersion trimming in a reconfigurable wavelength selective switch," *J. Lightw. Technol.*, vol. 26, no. 1, pp. 73–77, Jan. 2008.
- [24] K. Suzuki, K. Seno, and Y. Ikuma, "Application of waveguide/free-space optics hybrid to ROADM device," *J. Lightw. Technol.*, vol. 35, no. 4, pp. 596–606, Feb. 2017.
- [25] K. Seno *et al.*, "Demonstration of channelized tunable optical dispersion compensator based on arrayed waveguide grating and liquid crystal on silicon," *Opt. Express*, vol. 18, pp. 18565–18579, 2010.
- [26] D. Sinefeld, S. B. Ezra, and D. M. Marom, "Nyquist-WDM filter shaping with a high-resolution colorless photonic spectral processor," *Opt. Lett.*, vol. 38, no. 17, pp. 3268–3271, 2013.
- [27] M. Nakajima *et al.*, "Multilane photonic spectral processor integrated in spatial and planar optical circuit for space division multiplexing network," *J. Lightw. Technol.*, vol. 36, no. 2, pp. 309–317, Jan. 2018.
- [28] S. T. Cundiff and A. M. Weiner, "Optical arbitrary waveform generation," *Nature Photon.*, vol. 4, pp. 760–766, 2010.
- [29] L. Zhuang, C. G. H. Roeloffzen, M. Hoekman, K.-J. Boller, and A. J. Lowery, "Programmable photonic signal processor chip for radiofrequency applications," *Optica*, vol. 2, pp. 854–859, 2015.



- [30] Y. Sakurai *et al.*, "LCOS-based wavelength blocker array with channel-by-channel variable center wavelength and bandwidth," *IEEE Photon. Technol. Lett.*, vol. 23, no. 14, pp. 989–991, Jul. 2011.
- [31] N. K. Fontaine *et al.*, "Programmable gain equalizer for multicore fiber amplifiers," in *Proc. Opt. Fiber Commun. Conf.*, San Francisco, CA, USA, 2014, Paper Th5C.5.
- [32] M. Nakajima *et al.*, "Over-100-spatial-channel programmable spectral processor for SDM signal monitoring," in *Proc. Opt. Fiber Commun. Conf.*, San Diego, CA, USA, 2018, Paper W1E.2.
- [33] Y. Ikuma, K. Suzuki, N. Nemoto, E. Hashimoto, O. Moriwaki, and T. Takahashi, "Low-loss transponder aggregator using spatial and planar optical circuit," *J. Lightw. Technol.*, vol. 34, no. 1, pp. 67–72, Jan. 2016.
- [34] K. Seno *et al.*, "Spatial beam transformer for wavelength selective switch consisting of silica-based planar lightwave circuit," in *Proc. Opt. Fiber Commun. Conf.*, Los Angeles, CA, USA, 2012, Paper JTh2A.5.
- [35] K. Suzuki *et al.*, "Wavelength selective switch for multi-core fiber based space division multiplexed network with core-by-core switching capability," in *Proc. 21st Optoelectron. Commun. Conf./Int. Conf. Photon. Switching*, Niigata, Japan, 2016, Paper WF1-2.
- [36] Y. Sakamaki, K. Shikama, Y. Ikuma, and K. Suzuki, "Wavelength selective switch array employing silica-based waveguide frontend with integrated polarization diversity optics" *Opt. Express*, vol. 25, pp. 19946–19957, 2017.
- [37] B. Chomczyk, *Planning Fiber Optic Networks*. New York, NY, USA: McGraw-Hill, 2009.
- [38] J. H. Lee, D. K. Jung, C. H. Kim, and Y. C. Chung, "OSNR monitoring technique using polarization-nulling method," *IEEE Photon. Technol. Lett.*, vol. 13, no. 1, pp. 88–90, Jan. 2001.
- [39] R. Adams, M. Rochette, T. T. Ng, and B. J. Eggleton, "All-optical in-band OSNR monitoring at 40 Gb/s using a nonlinear optical loop mirror," *IEEE Photon. Technol. Lett.*, vol. 18, no. 3, pp. 469–471, Feb. 2006.
- [40] Y. Yu, B. Zhang, and C. Yu, "Optical signal to noise ratio monitoring using single channel sampling technique," *Opt. Express*, vol. 22, pp. 6874–6880, 2014.
- [41] J. Thrane, J. Wass, M. Piels, J. C. M. Diniz, R. Jones, and D. Zibar, "Machine learning techniques for optical performance monitoring from directly detected PDM-QAM signals," *J. Lightw. Technol.*, vol. 35, no. 4, pp. 868–875, Feb. 2017.
- [42] A. Annoni and F. Morichetti, "Enhancing the sensitivity of interferometer based in-band OSNR monitoring by narrow band filtering," *J. Lightw. Technol.*, vol. 31, no. 9, pp. 1447–1453, May 2013.
- [43] J.-Y. Yang, Y. Akasaka, and M. Sekiya, "Investigation of interferometric in-band OSNR monitor for monitoring nyquist-shaped 400G DP-QPSK superchannels," in *Proc. 2014 Photon. Conf.*, San Diego, CA, USA, 2014, pp. 304–305.

**Mitsumasa Nakajima** (M'15) received the B.E. degree in applied physics from the Science University of Tokyo, Tokyo, Japan, in 2008, and the M.E. and Ph.D. degrees in material science from the Tokyo Institute of Technology, Tokyo, Japan, in 2010 and 2015, respectively. In 2010, he joined Nippon Telegraph and Telephone (NTT) Microsystem Integration Laboratories, where he was involved in the development of MEMS micromirrors for optical switch applications. He is currently with NTT Device Technology Laboratories, Atsugi, Japan. He is the author of more than 40 research articles. His research interests include ferroelectric materials and their applications, optical circuit design, and their application to optical signal processing. He was a recipient of the Young Engineer Award from the Institute of Electronics, Information and Communication Engineers (IEICE) of Japan in 2013. He is a Member of the IEICE and the Japan Society of Applied Physics.

**Kenya Suzuki** (M'00) received the B.E. and M.E. degrees in electrical engineering and the Dr. Eng. degree in electronics engineering from the University of Tokyo, Tokyo, Japan, in 1995, 1997, and 2000, respectively. He joined Nippon Telegraph and Telephone (NTT) in 2000. From September 2004 to September 2005, he was a Visiting Scientist with the Research Laboratory of Electronics, Massachusetts Institute of Technology. From 2008 to 2010, he was with NTT Electronics Corporation, Ibaraki, Japan, where he was involved in the development and commercialization of silica-based waveguide devices. Since 2014, he has been a Guest Chair Professor with the Tokyo Institute of Technology, Meguro, Japan. He is currently with NTT Device Technology Laboratories, Atsugi, Japan. His research interests include optical circuit design and optical signal processing. He was a recipient of the Young Engineer Award from the Institute of Electronics, Information and Communication Engineers (IEICE) of Japan in 2003. He is a Member of the IEICE and the Physical Society of Japan.

**Kazunori Seno** received the B.E. and M.E. degrees in material engineering from Tohoku University, Sendai, Japan, in 2004 and 2006, respectively. In 2006, he joined Nippon Telegraph and Telephone (NTT) Photonics Laboratories, Kanagawa, Japan, where he was engaged in the research on optical devices based on spatial and planar optical circuit technology. From 2014 to 2016, he was engaged in the development of a photonic transport network system with NTT Network Service Systems Laboratories, Musashino, Japan. He is currently a Senior Research Engineer with NTT Device Technology Laboratories, Atsugi, Japan. He is a Member of the Institute of Electronics, Information and Communication Engineers of Japan.

**Ryoichi Kasahara** received the B.S. degree from The University of Electro-Communications, Tokyo, Japan, in 1995, and the M.S. degree from Tohoku University, Sendai, Japan, in 1997. In 1997, he joined Nippon Telegraph and Telephone (NTT) Opto-electronics Laboratories, Ibaraki, Japan, where he was involved in research on silica-based planar lightwave circuits, including thermo-optic switches and arrayed-waveguide grating multiplexers, and integrated optoelectrical receiver modules. He is currently with NTT Device Technology Laboratories, Kanagawa, Japan, where he has been involved in the research and development of the fabrication technologies of optical dielectric waveguide devices. He is a Member of the Institute of Electronics, Information, and Communication Engineers of Japan and the Japan Society of Applied Physics.

**Takashi Goh** (M'11) received the B.S. and M.S. degrees in electronics and communication engineering from Waseda University, Tokyo, Japan, in 1991 and 1993, respectively. In 1993, he joined Nippon Telegraph and Telephone (NTT) Opto-electronics Laboratories, Ibaraki, Japan, where he was involved in research on silica-based planar lightwave circuits, such as thermo-optic switches and arrayed-waveguide grating multiplexers. From 2002 to 2004, he was engaged in the development of optical communications systems, including reconfigurable add-drop multiplexing systems, with NTT Innovation Laboratories, Yokosuka, Japan. He is currently with NTT Device Technology Laboratories, Atsugi, Japan, where he has been involved in the research and development of optical devices, including advanced modulators and Nyquist filters for high-speed transmission and optical signal processing. He is a Member of the Institute of Electronics, Information, and Communication Engineers of Japan and the Japan Society of Applied Physics.

**Yutaka Miyamoto** (M'93) was born in Tokyo, Japan, on December 8, 1963. He received the B.E. and M.E. degrees in electrical engineering from Waseda University, Tokyo, Japan, in 1986 and 1988, respectively, and the Dr. Eng. degree in electrical engineering from Tokyo University, Tokyo, Japan. In 1988, he joined Nippon Telegraph and Telephone (NTT) Transmission Systems Laboratories, Yokosuka, Japan, where he was engaged in research and development of high-speed optical communications systems, including the first 10-Gbit/s terrestrial optical transmission system (FA-10G) using EDFA inline repeaters. He then joined NTT Electronics Technology Corporation, where, between 1995 and 1997, he was engaged in the planning and product development of high-speed optical modules operating at 10 Gbit/s and higher. Since 1997, he has been with NTT Network Innovation Laboratories, where he has engaged in research and development of optical transport technologies offering channel rates from 40 Gbit/s to 1 Tbit/s. He is currently a Senior Distinguished Researcher and the Director of the Innovative Photonic Network Research Center, NTT Network Innovation Laboratories. His current research interests include scalable high-capacity optical transport systems with advanced modulation formats, digital signal processing, optical preprocessing, and space division multiplexing. He is a Fellow of the Institute of Electronics, Information, and Communication Engineers of Japan.

**Toshikazu Hashimoto** received the B.S. and M.S. degrees in physics from Hokkaido University, Hokkaido, Japan, in 1991 and 1993, respectively. Since 1993, he has been with Nippon Telegraph and Telephone Laboratories, Atsugi, Japan, where he is researching hybrid integration of semiconductor lasers and photodiodes on silica-based planar lightwave circuits and the wavefront matching method. He is a Member of the Institute of Electronics, Information and Communication Engineers of Japan, the Physical Society of Japan, and the Optical Society.